

# A Deep Study of the High-Energy Transient Sky

**White Paper submitted to ESA Voyage 2050 Call**

**DEEPER & BROADER:  
FUTURE OBSERVATIONS IN THE X-/GAMMA-RAY BAND  
OF KNOWN AND UNKNOWN EXPLOSIVE TRANSIENTS**

**Contact Person:**

Name: Cristiano Guidorzi

Dept. Physics and Earth Science, University of Ferrara, Italy

Email: [guidorzi@fe.infn.it](mailto:guidorzi@fe.infn.it)

Phone: +39-0532-974368

**Proposing team:** C. Guidorzi<sup>1</sup>, F. Frontera<sup>1,2</sup>, G. Ghirlanda<sup>3,4</sup>, G. Stratta<sup>2</sup>, C.G. Mundell<sup>5</sup>, E. Virgili<sup>1</sup>, P. Rosati<sup>1</sup>, E. Caroli<sup>2</sup>, L. Amati<sup>2</sup>, E. Pian<sup>2</sup>, S. Kobayashi<sup>6</sup>, G. Ghisellini<sup>3</sup>, C. Fryer<sup>7</sup>, M. Della Valle<sup>8,9,10</sup>, R. Margutti<sup>11</sup>, M. Marongiu<sup>1,10</sup>, R. Martone<sup>1,10</sup>, R. Campana<sup>2</sup>, F. Fuschino<sup>2</sup>, C. Labanti<sup>2</sup>, M. Orlandini<sup>2</sup>, J. B. Stephen<sup>2</sup>, S. Brandt<sup>12</sup>, R. Curado da Silva<sup>13,14</sup>, P. Laurent<sup>15</sup>, R. Mochkovitch<sup>16</sup>, E. Bozzo<sup>17</sup>, R. Ciolfi<sup>18,19</sup>, L. Burderi<sup>20</sup>, T. Di Salvo<sup>21</sup>

<sup>1</sup> Department of Physics and Earth Science, University of Ferrara, Via Saragat 1, I-44122 Ferrara, Italy

<sup>2</sup> Observatory of Astrophysics and Space Sciences, National Institute of Astrophysics (INAF), Via Gobetti 101, 40129 Bologna, Italy

<sup>3</sup> INAF – Osservatorio Astronomico di Brera, via E. Bianchi 46, I-23807 Merate, Italy

<sup>4</sup> Dipartimento di Fisica G. Occhialini, Università di Milano Bicocca, Piazza della Scienza 3, I-20126 Milano, Italy

<sup>5</sup> Department of Physics, University of Bath, Claverton Down, Bath, BA2 7AY, UK

<sup>6</sup> Astrophysics Research Institute, Liverpool John Moores University, Liverpool, L3 5RF, UK

<sup>7</sup> Los Alamos National Laboratory - New Mexico 87545, USA

<sup>8</sup> Capodimonte Astronomical Observatory, INAF-Napoli, Salita Moiariello 16, 80131-Napoli, Italy

<sup>9</sup> Instituto de Astrofísica de Andalucía (IAA-CSIC), Glorieta de la Astronomía, s/n, 18008, Granada, Spain

<sup>10</sup> International Center for Relativistic Astrophysics, Piazzale della Repubblica 2, I-65122 Pescara, Italy

<sup>11</sup> Center for Interdisciplinary Exploration and Research in Astrophysics and Department of Physics and Astronomy, Northwestern University, 2145 Sheridan Road, Evanston, IL 60208-3112, USA

<sup>12</sup> Technical University of Denmark, National Space Institute, Elektrovej, Denmark

<sup>13</sup> LIP-Laboratório de Instrumentação e Física Experimental de Partículas, Portugal

<sup>14</sup> Physics Department, University of Coimbra, Coimbra, Portugal

<sup>15</sup> IRFU, CEA, Université Paris-Saclay, F-91191 Gif-sur-Yvette, France

<sup>16</sup> Sorbonne Université, CNRS, UMR 7095, Institut d'Astrophysique de Paris, 98 bis bd Arago, 75014 Paris, France

<sup>17</sup> Department of Astronomy, University of Geneva, chemin d'Ecogia 16, 1290 Versoix, Switzerland

<sup>18</sup> INAF, Osservatorio Astronomico di Padova, Vicolo dell'Osservatorio 5, I-35122 Padova, Italy

<sup>19</sup> INFN, Sezione di Padova, Via Francesco Marzolo 8, I-35131 Padova, Italy

<sup>20</sup> Dipartimento di Fisica, SP Monserrato-Sestu, Università degli Studi di Cagliari, km 0.7, 09042 Monserrato, Italy

<sup>21</sup> Dipartimento di Fisica e Chimica, Università degli Studi di Palermo, Via Archirafi 36, 90123 Palermo, Italy

## Executive Summary

The detection of gravitational and electromagnetic (EM) radiation from the binary neutron star (BNS) merger GW 170817 in 2017 heralded the beginning of the multi-messenger study of the transient sky. Coming decades will establish the exploration of the gravitational wave (GW) Universe over a broad frequency range by ground and space interferometers. Meanwhile, an armada of wide-field, high-cadence and sensitive surveys will span the EM spectrum from radio (SKA), through optical (LSST) and up to X/ $\gamma$ -ray (e.g. THESEUS, accepted by ESA for a phase A study), and TeV (CTA), as well as particle-detectors such as those in the high-energy neutrino window (e.g., IceCube-Gen2, KM3NeT). This towering effort will enable the study of events characterised by strong gravity effects, relativistic shocks, and particle acceleration processes over a broad mass, time, and distance scales. Not only will they address open issues of astrophysics, cosmology, and fundamental physics (e.g., formation of compact binaries, the equation of state of matter at nuclear densities, nucleosynthesis of heavy elements, cosmic-ray production, the nature of dark matter and the cosmological parameters), but they will also significantly boost the discovery rate of known and unknown rare classes of transient sources throughout the Universe. Among the numerous classes of transients, gamma-ray bursts (GRBs) have direct links with most of the topics mentioned above. Accurate and systematic GRB polarisation measurements can probe the magnetic field intensity and configuration, which is key to understanding relativistic jet formation and shock acceleration physics. Other totally unexpected classes that were discovered only a few years ago are fast radio bursts (FRBs), fast blue optical transients (FBOTs), and other unidentified high-energy transients. The keV-to-MeV energy band is ideally suited to help explore high-energy, non-thermal phenomena.

In this white paper we discuss how these topics, summarised in the key science questions below, can be addressed by a mission called ASTENA (Advanced Surveyor of Transient Events and Nuclear Astrophysics). Its payload combines two instruments: (i) an array of wide-field monitors with imaging, spectroscopic, and polarimetric capabilities (WFM-IS); (ii) a narrow field telescope (NFT) based on a Laue lens operating in the 50–600 keV range with unprecedented angular resolution, polarimetric capabilities, and sensitivity. With respect to THESEUS - aiming at fully exploiting GRBs for early Universe and multi-messenger astrophysics - ASTENA will carry out a deeper study of the *physics* of their prompt and afterglow emission. Building on the foundation of the THESEUS X-Gamma-ray Imaging Spectrometer (XGIS), ASTENA WFM-IS will have a higher effective area (by a factor of 6), thus providing a substantial step forward for timing, spectroscopy and polarimetry of GRB prompt emission. The superior 1-arcmin angular resolution of ASTENA WFM-IS is also crucial to perform the NFT follow up of the discovered events.

## Key Science Questions

- **What is the GRB prompt emission mechanism? What role do magnetic fields have in the jet formation, propagation, energy dissipation, and shock acceleration physics?**
- **Electromagnetic counterparts of GW events: what are the jet structure and demographics of short GRBs associated with the merging of BNS?**
- **What mechanism powers the transient, long-lived hard X/soft  $\gamma$ -ray emission that characterises GRB afterglows?**
- **What sources lie behind the number of known transients and unknown X/ $\gamma$ -ray transients that have recently been discovered?**

## GRB prompt emission mechanism and magnetic field's role

Technological advancement over the past two decades has revolutionised our understanding of the nature of GRBs (see, e.g., review by [1]), propelling them from mysterious, poorly localised and relatively unstudied, high-energy flashes of unknown origin to the focus of a global scientific community whose efforts have confirmed GRBs to represent the endpoints of stellar evolution and compact binary mergers, drivers of ultrarelativistic plasma outflows and, possibly, key cosmic producers of heavy metals such as gold - all at vast cosmological distance [2] and discovered, localised and followed up in real time.

Despite this rapid progress, the field is in its infancy and fundamental questions on the origin, physics and impact of GRBs remain. The mechanism responsible for the  $\gamma$ -ray prompt emission, i.e. the GRB itself, is not yet understood and in many cases cannot be explained with pure optically thin synchrotron. In particular, we do not know how the ultra-relativistic jet is formed near the progenitor, how it propagates through the stellar interior, and the origin and configuration of the associated magnetic field [3], which is a key ingredient for understanding the emission process and the shock acceleration physics [4]. The physical processes, the energy dissipation mechanism, the magnetisation content, and the involved jet geometry that rule the prompt emission can uniquely be investigated through **prompt hard X/ $\gamma$ -ray polarisation measurements** (e.g., [5]).

Novel instruments on a new generation of fully autonomous, robotic optical telescopes have made rapid early time optical afterglow polarimetry a reality [6–8], revealing a wide range of polarisation properties and confirming the presence of entrained, ordered magnetic fields in some GRB jets. The detection of optical polarisation has regenerated interest in new high-energy polarisation missions (e.g. ESA-XIPE, NASA-IXPE, POLAR), despite early controversies and accepted technical challenges in accurately calibrating systematics at  $\gamma$ -ray energies. The first claim of polarised prompt optical light [9] provides further motivation. To date, no GRB has yet been observed in polarised light from high-energy  $\gamma$ -rays through X-ray, optical and to radio across prompt, early and late afterglow. Such a dataset would provide unprecedented insight into the physics of GRBs. In addition, although technically more challenging,  $\gamma$ -ray polarimetry probes directly the prompt emission mechanism and its magnetic field configuration.

According to a recent review [10], previous/current missions (*CGRO*, *RHESSI*, *INTEGRAL*, *IKAROS*, *Astrosat*) reported prompt  $\gamma$ -ray polarisation measurements for ten GRBs. However, the results are highly uncertain for some events, and others have a limited statistical significance ( $< 4\sigma$ ). Recently, polarisation results have been obtained for 5 bright GRBs (161218A, 170101A, 170127C, 170206A, 170114A) with the POLAR experiment aboard the China's spacelab Tiangong-2 [11]. The systematic errors are certainly better controlled, but the statistical significance, also due to the low polarisation found, is still at about  $3\sigma$  level. Indeed, the authors state that their analysis does not allow to fully reject the hypothesis that the analysed GRBs are not polarised, even though the observed changes in the polarisation angle suggest a strong temporal evolution as a possible explanation for the low time-averaged polarisation degree. On the basis of the available data, it is difficult to draw definitive conclusions about the underlying physics and emission mechanisms, like the presence of a globally ordered magnetic field in the emission region (e.g., [12]) or the presence of a randomly structured field (e.g., [13]). About the emission mechanisms, from the current polarisation measurements it is still not possible to discriminate, e.g., between synchrotron in a uniform B-field or in a random B-field, or, for example, the possible presence of a Compton drag. As for the jet structure and geometry, depending on the emission mechanism and on the origin

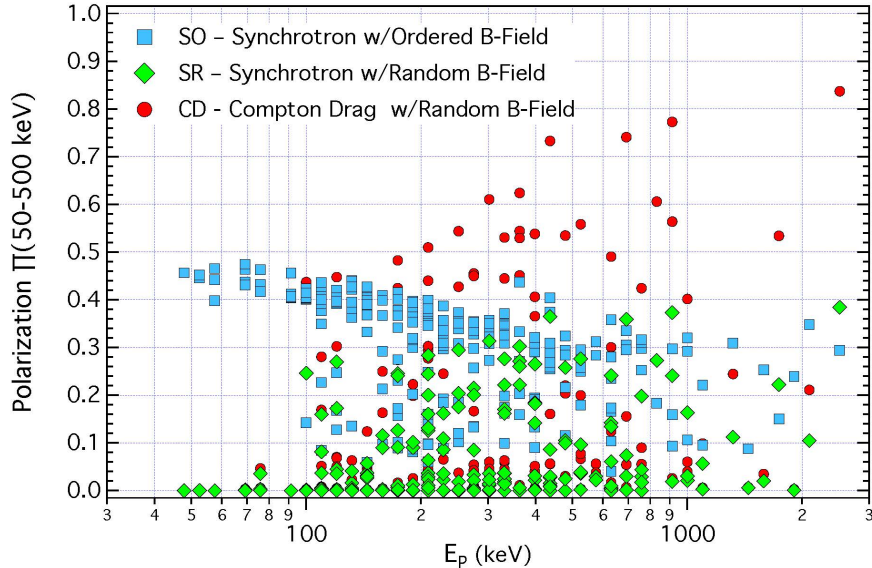


Figure 1: Distribution of the predicted polarisation level as a function of the intrinsic peak energy  $E_p$  for three different emission models. The distribution is that reported by McConnell [10], that was derived by means of a Montecarlo simulation of 10,000 GRB jets with parameter distributions described by Toma et al. [14].

and configuration of the magnetic field, the polarisation level may depend on the viewing angle, i.e. the angle between the line of sight and the jet axis [13]. To draw conclusions about these open issues, one should measure the hard X/ $\gamma$ -ray polarisation of a significant sample and correlate with other key properties. For example Toma et al. [14] derived how the distribution of the polarisation level depends on the intrinsic peak energy  $E_p$  of the  $EF(E)$  spectrum for three different models (see Fig. 1). To further test some models, it is equally important to carry out time-resolved polarisation measurements: for instance, the internal-collision-induced magnetic reconnection and turbulence (ICMART) model predicts decreasing  $\gamma$ -ray polarisation degree and  $E_p$  with time throughout each individual broad  $\gamma$ -ray pulse [15].

In addition, time-resolved polarisation measurements of GRB prompt emission make it possible to test the weak equivalence principle (WEP) with unprecedented sensitivity: should the WEP be violated, the temporal evolution of the polarisation angle would depend on both photon energy and GRB distance [16].

The ASTENA WFM-IS, thanks to its specific capability as a polarimeter, its very large detection area and broad passband, is expected to provide accurate information about the polarisation level of a large sample of GRBs, also determining its temporal and energy dependence. We estimated the minimum detectable polarisation (MDP) as a function of photon energy, for a typical long GRB with a fluence of  $\sim 10^{-4}$  erg cm $^{-2}$ : as shown in Fig. 2, the MDP is  $< 10\%$  for  $E < 300$  keV, and  $< 30\%$  for  $E < 600$  keV. The broad passband is key to cover  $E_p$  for most GRBs, not only because most of the energy is emitted around  $E_p$ , but also because it makes it possible to discriminate between competing models based on the polarisation degree vs.  $E_p$  distribution, and to test predictions on spectro-polarimetric evolution patterns.

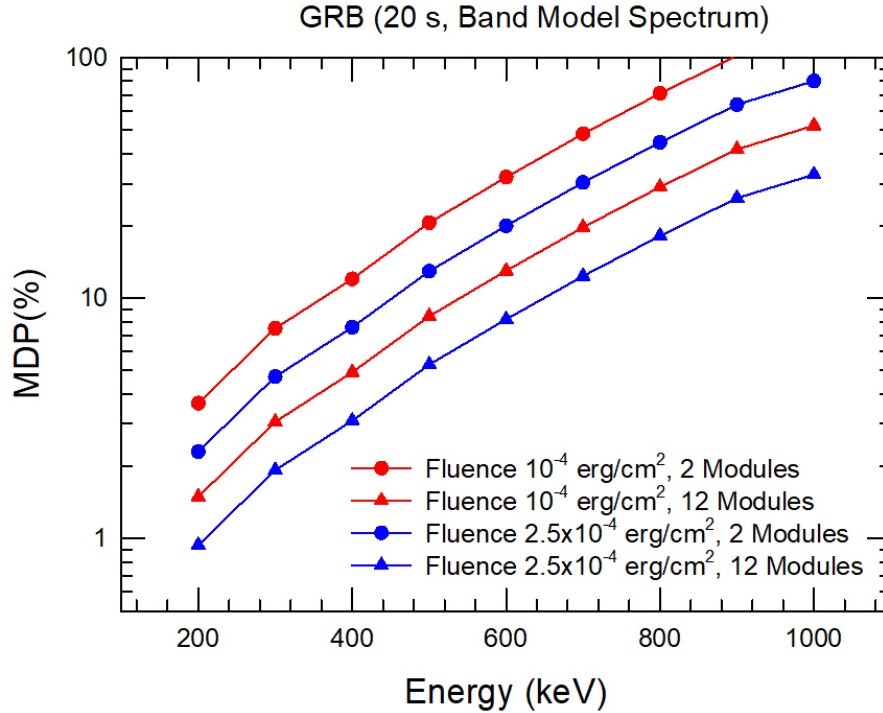


Figure 2: Minimum detectable polarisation with ASTENA WFM-IS for a 20-s long GRB, with different fluence values, and for two different number of modules. The GRB spectrum is described by the Band function with typical values ( $\alpha = -1$ ,  $\beta = -2.3$ ,  $E_p = 300$  keV).

## Electromagnetic Counterparts of Gravitational Wave Events

The observation of the gravitational wave event GW 170817 by the LIGO-Virgo Collaboration (LVC) and the discovery of short GRB 170817A  $\sim 1.7$  s later and positionally consistent with the location uncertainty ( $31 \text{ deg}^2$ ) of the GW event has ushered in the multi-messenger astronomy era [17]. Finding the EM counterpart of a GW event is crucial (1) to provide independent confirmation of the astrophysical origin of the GW trigger, especially for GW events with low significance (e.g., subthreshold triggers), (2) to accurately determine the position in the sky, and therefore (3) to allow for the host galaxy identification and redshift determination. As a consequence, this information can break the degeneracy between position in the sky and other observables, both extrinsic (binary inclination and GW polarisation angles, distance) and intrinsic (orbital angular momentum, spins [18]). In addition, it makes it possible to independently estimate the Hubble constant (e.g., [19]) and to investigate fundamental physics, like the Lorentz Invariance violation foreseen in quantum gravity theories (e.g., [20]).

On the basis of the results obtained from the detection of the short GRB 170817A and the observing campaign that led to the discovery of the kilonova (KN) associated with GW 170817 in the outskirts of the galaxy NGC 4993 at a distance of 40 Mpc from the Earth, a few important properties are worth mentioning: a) GRB 170817A is sub-luminous ( $\sim 1 \times 10^{47} \text{ erg s}^{-1}$ ) [21]; b) it is softer than typical short GRBs (sGRBs), as demonstrated by its non detection (upper limit of  $10^{-7} \text{ erg cm}^{-2} \text{ s}^{-1}$  in 0.2-5 MeV) with the very large effective area High Energy (HE) instrument aboard the Insight-HXMT mission [22]; c) a very rough localisation accuracy of the event (90% probability region of about 1800 square degrees) obtained with the GBM instrument

aboard the *Fermi* satellite. This very rough localisation accuracy, combined with the low hard X-ray flux, prevented an accurate spectral analysis and an immediate multiwavelength follow-up of GRB 170817A for the study of the afterglow emission.

The broadband study of the afterglow of GRB 170817A allowed us to model the jet geometry, the kinetic energy and bulk velocity angular structure, raising the following questions: is the jet structure universal? Which parameters are involved? To answer these, it is worth noting that the presence of a universally structured jet, whose origin is directly related to the central engine and its interaction with the ambient medium (e.g. [23]), could also be assessed through prompt emission observations and population studies [24, 25].

All the above sGRB properties and instrument limitations could be ideally addressed with an instrument with a much more sensitive wide-FOV monitor, a very broad energy passband that extends to low X-ray energies ( $\sim 1$  keV), and with spectroscopic and possibly polarimetric capabilities. The WFM-IS proposed by us matches all these requirements. Compared with THESEUS-XGIS, which operates in the same broad energy band, the WFM-IS has larger FOV ( $\sim 2$  vs.  $1.5$  sr), significantly larger effective area (by a factor of  $\sim 6$ ), and most importantly better point source localisation accuracy ( $1$  vs.  $5$  arcmin), which is crucial to allow for a rapid followup of focusing telescopes, such as the NFT.

In the 2030's, 3G GW detectors such as the Einstein Telescope (ET) and the Cosmic Explorer (CE) will be operational. The ET will detect  $> 10^4$  yr $^{-1}$  BNS mergers out to  $z \sim 2$  [26], of which a few tens will also be detected with THESEUS-XGIS as sGRBs. On the optical side, LSST will not detect KN emission beyond  $z \sim 0.5$ . Therefore, the combination of larger effective area and broad band of WFM-IS is essential to fully exploit the potential of ET+CE for prompt localisation and characterisation of the associated EM emission for more BNS mergers. This, in turn, will boost the population study. The distribution of observed GW-EM delays, combined with the spectral characterisation and  $\gamma$ -ray luminosity of the associated sGRB, will further constrain the jet geometry, structure, and finally the formation channel(s) of these compact binary systems.

The mentioned GRB properties are those found in the case of a GW event due to a BNS merger. NS-BH are expected to produce different EM counterparts (GRB, kilonova, afterglow – e.g., [27]). However, their luminosity and evolutionary timescales are still observationally unexplored.

Lastly, the Laser Interferometer Space Antenna (LISA), that will be observing GWs in the millihertz band, will detect thousands of stellar-mass binary black hole (BBH) mergers, hundreds of which will be discovered years before coalescence. It will predict the time of merging with  $< 10$  s uncertainty and  $< 1$  deg $^2$  position error [28]. A sensitive, broadband, X/ $\gamma$ -ray monitor with a sufficient FOV such as the ASTENA WFM-IS is key to monitor a possible prompt EM counterpart.

### Hard X-ray spectrum and polarisation of GRB afterglows

Thanks to the *BeppoSAX* mission that discovered GRB afterglows and the *Swift* mission that initiated the systematic study of the early afterglow, we have a very consolidated knowledge of the temporal and spectral behaviour of the low energy ( $< 10$  keV) afterglow (see, e.g., [1, 29]). However, due to the limited sensitivity of the current instrumentation, at higher energies the afterglow temporal and spectral behaviour is an almost uncharted territory. High energy X-ray measurements have been obtained only by the *BeppoSAX* Phoswich Detection System (PDS) [30], *NuSTAR* [31], or *INTEGRAL* [32]. The PDS telescope detected the high energy afterglow of GRB 990123, one of the brightest GRBs observed with *BeppoSAX*. The afterglow was detected up to 60 keV, with a power-law decay in the 15–28 keV that was consistent with that found in the 2–10 keV band (slope

$\alpha = 1.46 \pm 0.04$ ) at least up to 12 hrs after the event. Concerning the afterglow spectrum between 6 and 11 hrs from the GRB onset, it was found that from 0.6 to 60 keV it was well fit with an absorbed power-law with the multiwavelength spectral energy distribution (SED) shown in Fig. 3. Corsi et al. [33] discussed the *BeppoSAX* results finding that, while the temporal and spectral behaviour of the optical afterglow is consistent with synchrotron with cooling frequency between the optical and the X-rays as long as the 2–10 keV data are considered, this is no more the case when the spectrum is extended up to 60 keV. In this case an Inverse Compton (IC) scattering was proposed to explain the *BeppoSAX* results. The importance of the hard X-ray detection for establishing the afterglow emission mechanism at play is confirmed by the results obtained by Kouveliotou et al. [31], who detected the hard X-ray afterglow from GRB 130427A with *NuSTAR*. The result was that "the *NuSTAR* data are essential in constraining the shape of the broadband spectra". In this case the *NuSTAR* power-law spectrum and decay law are still consistent with a synchrotron emission mechanism of the GRB afterglow. Analogous results and conclusions were also obtained for the bright GRB 120711A [32].

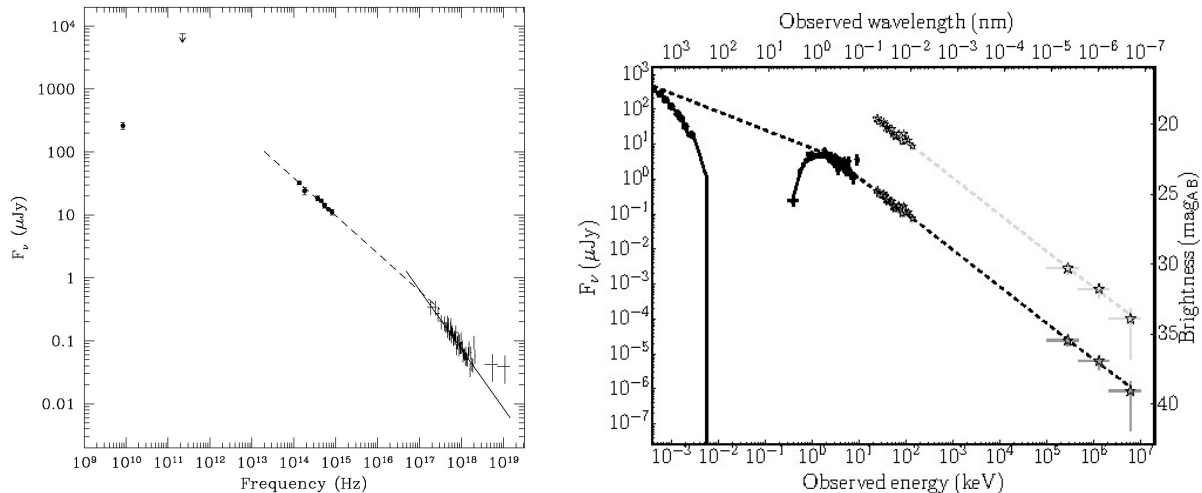


Figure 3: *Left*: spectral Energy Distribution (SED) of the afterglow emission of GRB 990123. Reprinted from [30]. *Right*: same for the afterglow of GRB 120711. The same spectral regime spans the X-ray-to-GeV energy range (reprinted from [32]).

For a few GRBs, whose 0.3–10 keV afterglow was found to be exceptionally soft (power-law photon index  $\Gamma_X > 3$ ), Moretti et al. [34] found that an additional, hard X-ray component of unknown origin and modelled as a hard power-law, was required by the data. Such a component could be more ubiquitous than what has been observed with *Swift*-XRT; only when the dominant component is particularly soft, as in the case of these GRBs, the hard one would become detectable.

In the cases of some late X-ray afterglows, the combination of (i) slow decay, (ii) very soft ( $\Gamma_X > 3$ , inconsistent with a pure synchrotron origin), (iii) larger-than-average intrinsic absorption, and (iv) very long ( $T_{90} > 1000$  s) prompt  $\gamma$ -ray emission, was observed [35]. The negligible chance probability of a random combination of all these rare properties suggested that the extremely soft X-ray emission could be due to reprocessing by the complex circumburst environment sculpted by the progenitor prior to the final explosion. A hard X/ $\gamma$ -ray characterisation of the afterglow is missing and it would help test this interpretation.

*Fermi*/LAT unveiled the presence of the afterglow emission at very high energies [36, 37]. So far it detected long-lived emission in the 100 MeV–100 GeV range for almost 200 GRBs [38]. Combining *Swift*/XRT and LAT data, Ajello et al. [39] found that the presence of a synchrotron cooling break between X-rays and GeV can explain the non-detection by LAT of relatively bright X-ray afterglows, whereas LAT-detected GRBs are mostly consistent with a synchrotron spectrum whose cooling break lies either below X-rays or above the LAT passband (see Fig. 4). This, in turn, suggests that LAT-detected GRBs occur in wind-profile, low-density circumburst environments. No evidence is found for a dominant synchrotron self-Compton (SSC) component in the LAT range (with implications on the relative strength of the shock microphysics parameters describing the magnetic field vs. electron energy), where the possibility remains that such an SSC component is detectable below 100 MeV.

These few observations clearly show the importance of filling the energetic gap between X-rays and the LAT passband in the afterglow study: this would help shed light on the nature of the very high-energy early afterglow and on the possible role of pairs [36, 40]. ASTENA, thanks to the unprecedented sensitivity of the Narrow Field Telescope (NFT) (see below) will be capable to measure the high energy spectrum and the polarisation of the afterglow emission of a large sample of GRBs, and thus to establish the underlying physics and the emission mechanisms in play (e.g., synchrotron photon energy, presence of a Compton or pair production component in addition to the synchrotron) and the corresponding parameters.

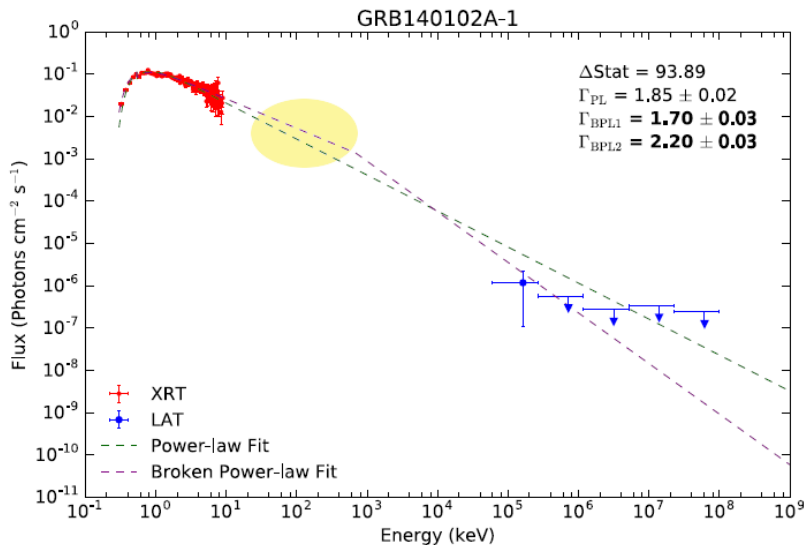


Figure 4: Example of a X-ray-to-GeV SED of the afterglow of GRB 140102A based on *Swift*/XRT and *Fermi*/LAT data. The yellow area highlights where ASTENA/NFT observations are key to constrain the presence of synchrotron cooling break (adapted from [39]).

### Low Luminosity GRBs

Low luminosity GRBs (*ll*GRBs) are a sub-population of long GRBs. They are single peaked, smooth and in most cases soft, with luminosity in the range  $10^{47}$ – $10^{49}$  erg, much lower than typical GRBs. Most of them (about a dozen) are associated with type Ic supernovae (SNe). The prototype of the *ll*GRBs is GRB 060218, from which evidence of a relativistic shock-breakout (SBO) of

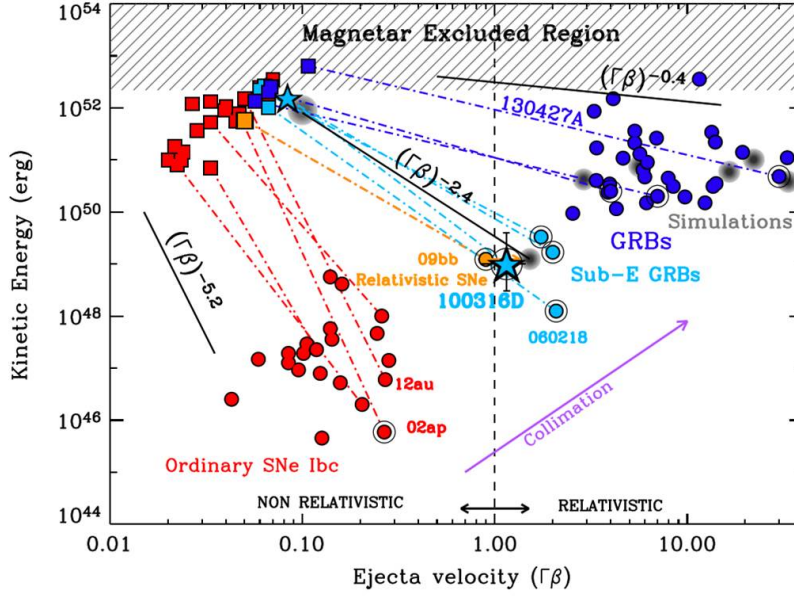


Figure 5: Kinetic energy behaviour of different classes of transient sources, i.e. ordinary SNe type Ibc, //GRBs and classical GRBs (reprinted from [43]).

the stellar envelope and the stellar wind was observed [41]. However, few of them do not have an associated SN, e.g., GRB 060505 [42]. These properties place //GRBs between the highly relativistic, collimated GRB explosions and the spherical, ordinary Type Ib/c SNe as it is shown in Figure 5 (reprinted from [43]), which compares the kinetic energy distribution (or profile) versus the outflow four-velocity for different classes of sources. As suggested by this figure and as it was discussed by Margutti et al. [43], the kinetic energy profile of //GRBs is intermediate between that of ordinary, non-relativistic SNe Ibc and that of classical GRBs. This behaviour of //GRBs calls for the presence of a central engine that drives a jet which either gets choked or is barely able to reach the star surface. In the relativistic SBO interpretation [44], three observables (duration, SBO energy, and SBO temperature) can be used to measure the SBO radius, thus making inferences on the progenitor's nature. In addition, the so-called relativistic SBO relation must be satisfied by the same observables:

$$\frac{t_{\text{bo}}^{\text{obs}}}{20\text{s}} \sim \left( \frac{E_{\text{bo}}}{10^{46}\text{erg}} \right)^{1/2} \left( \frac{T_{\text{bo}}}{50\text{keV}} \right)^{-2.68}.$$

This way, one can explain both typical long-soft events and less common, relatively short ( $\sim 30$  s) and hard ( $E_p \sim 50$  keV) ones, such as GRB 980425 [45, 46]. Alternatively, //GRBs could be the natural extension of cosmological GRBs in a universal structured jet scenario [24, 25].

All observed //GRBs are at low redshifts ( $\leq 1$ ). Due to their low luminosities, with the current instrumentation they could not have been detected from further out. However, taking into account the relatively small sampled volume, their inferred volumetric rate could be much larger than that of typical long GRBs [47–49]. So a much more sensitive wide field monitor than the current GRB instrumentation is needed to perform a sensitive sky survey of //GRBs.

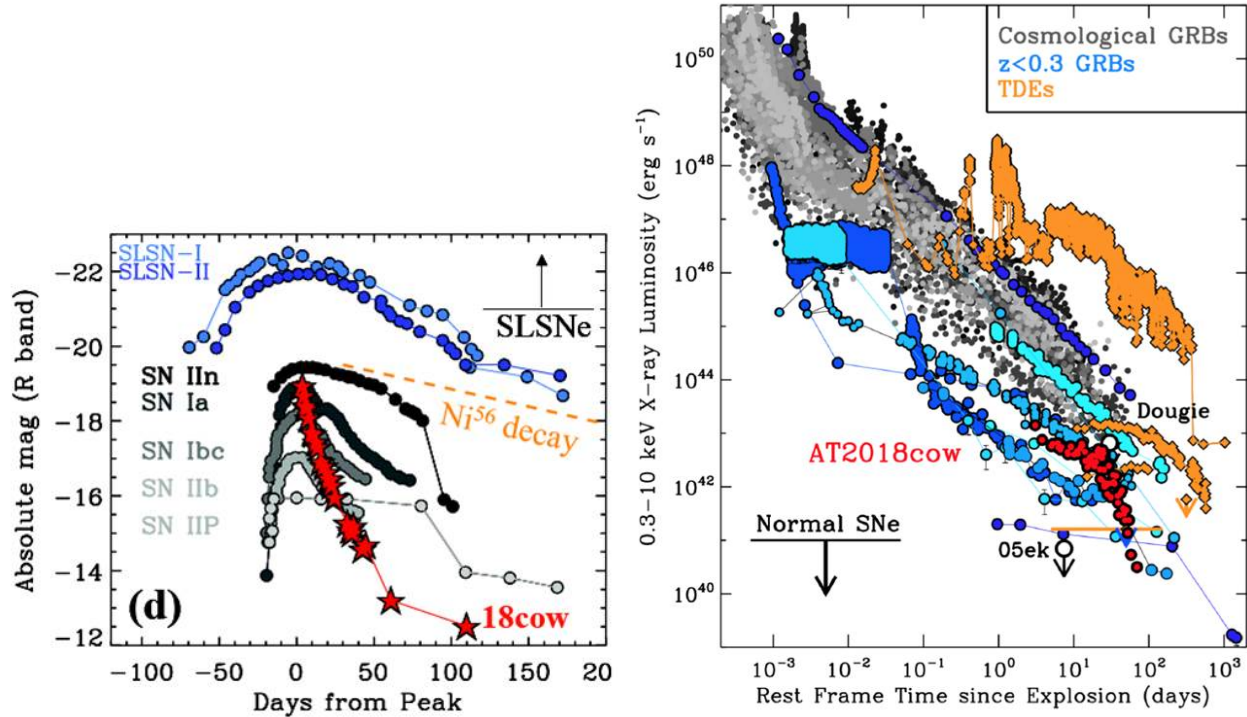


Figure 6: *Left*: Comparison of the optical light curve of AT2018cow with those of the various types of SNe. *Right*: Comparison of the X-ray fading of AT2018cow with those of GRBs and TDEs. Reprinted from Margutti et al. [54].

### Fast Blue Optical Transients

Fast blue optical transients (FBOTs) are likely a new class of transient sources [50], which typically show blue spectra, can be as luminous as SNe-Ibc ( $L_{\text{peak}} > 10^{43}$  erg/s), but evolve more rapidly ( $t_{\text{rise}} \ll 4$  days), in tension with the powering of  $^{56}\text{Ni}$  decay as prescribed by traditional SN models [51, 52]. At the moment only very few objects of this class have been detected in X-rays, and AT2018cow, discovered in the optical band [53], is by far the best studied yet, also thanks to its vicinity (60 Mpc). AT2018cow was found [54] to fade very rapidly, much more than all types of SNe (see left panel of Fig. 6) with a peak luminosity of about  $4 \times 10^{44}$  erg/s. Yet, from the star formation properties of the host dwarf galaxy and the site of AT2018cow within the host, a massive star origin is favoured [55]. Its X-ray counterpart, detected with the *Swift* XRT, *NuSTAR* and *INTEGRAL* [54], faded in the 0.5–10 keV band faster than typical GRB afterglows, more similar to that of tidal disruption events (TDEs; see right panel of Fig. 6). The very interesting peculiarity of AT2018cow in the X-ray band is its low-energy power-law spectrum that extends to hard X-rays with a very broad bump that fades away at  $\sim 20$  days. This feature is uncommon in transient objects.

AT2018cow is likely the prototype of a new class of transients that are expected to be detected in the optical band copiously thanks to the current and forthcoming wide-field surveys. Yet, the following questions remain unanswered: which is the progenitor of this class of transients? Are they related with GRBs or TDEs? In this case they should show a prompt emission, yet undetected. How common is the hard X-ray component and which is its origin?

Margutti et al. [54] propose as origin of the AT2018cow hard X-ray bump, at 7.7 days from the optical discovery, a Compton-disk reflection model. Only numerous detections in the future

and more sensitive hard X-ray observations can clarify the origin of the FBOT emission and their progenitors.

### Fast Radio Bursts

In addition to the possible class of the X/ $\gamma$ -ray counterparts of the FBOTs, another class of transient events could exhibit an associated X/ $\gamma$ -ray emission: fast radio bursts (FRBs). Discovered in 2007 [56], FRBs are still one of the most intriguing mysteries in astrophysics (see [57, 58] for recent reviews). They are very short ( $\gtrsim 1$  ms) and are distributed randomly over the sky. Although the number of FRBs publicly announced so far is still limited ( $\sim 80$  as of July 2019), there is no concentration of FRB in the Galactic plane, and thus they are very likely isotropically distributed over the sky. Their extragalactic origin is based on the detection of a repeating FRB (121102, [59]), that has allowed to accurately determine the FRB direction and thus its association with a persistent radio source [60], coincident with a bright star-forming region located in the outskirts of an irregular, low-metallicity dwarf galaxy with a redshift  $z = 0.193$  [61]. Very recently, the redshifts of two other non-repeating FRBs were obtained: FRB 180924 at  $z = 0.3214$  [62] and FRB 190523 at  $z = 0.66$  [63]. Meanwhile, another repeating FRB (180814) has been detected [64]. Their dispersion measures, if assumed to be produced mostly in the intergalactic medium, can be used as proxy of their distances: under this assumption, their luminosities are in the range  $10^{38}$ – $10^{43}$  erg/s, which are much lower than those found for GRBs, even *ll*GRBs. This fact would mean that FRBs are much less energetic than other astrophysical transients, and thus their counterparts are hardly detectable, unless they are many orders of magnitude more energetic than the FRBs themselves. Actually, controversial evidence was found of a putative *Swift* GRB spatially and temporally coincident with FRB 131104 [65], although no simultaneous X-/ $\gamma$ -ray counterparts to other even much radio brighter FRBs were found [66–68]. Several models that have been proposed in the literature so far, (e.g., [69–72] and references therein) do not exclude the possibility of  $\gamma$ -ray emission associated to FRBs. Therefore, it is very important to have a very sensitive instrument with imaging capabilities that can detect possible  $\gamma$ -ray counterparts of FRBs.

### Other Unknown High-Energy Transients

A number of extragalactic X-ray transients has been discovered in the latest years, with luminosities in the range  $10^{40}$ – $10^{46}$  erg/s and duration of several seconds to hours. Their origin remains mysterious and while several interpretations remain plausible, none of them appears to be convincing. Hereafter, we briefly review some of them as a few examples.

An X-ray flash was observed with  $L = 6 \times 10^{42}$  erg/s. It lasted 4000 s and was found in the elliptical galaxy M86 without any apparent hard X/ $\gamma$ -ray emission ([73]; see also [74, 75]). It could be the result of a tidal disruption of a white dwarf by an intermediate BH or an off-axis short GRB.

Ultraluminous X-ray flares with luminosities in the range  $10^{39}$ – $10^{41}$  erg/s were observed repeatedly from extragalactic X-ray sources, that otherwise look like compact X-ray binaries [76]. They showed a fast rise (about one minute), followed by  $\sim 10^3$ -s decay. Although the flaring and its energetic are reminiscent of Galactic magnetars, they are located in old stellar population regions.

Another X-ray transient was discovered serendipitously in the Chandra Deep Field-South [77], showing a comparable rise time, followed by a power-law decay. Its energy spectrum is modelled with a relatively hard power-law, with photon index  $\Gamma_X = 1.43_{-0.13}^{+0.23}$ . The peak luminosity lies in the range  $10^{44}$ – $10^{47}$  erg/s, depending on the unknown distance. While most of the previously known X-ray transients are ruled out, the following possible interpretations remain plausible: X-ray

afterglow of either (i) an off-axis sGRB or (ii) a *ll*GRB at  $z \gtrsim 2$  with no prompt emission below 20 keV; (iii) a highly beamed TDE of a white dwarf disrupted by an intermediate black hole. The estimated rate of these X-ray transients lies in the range from a few up to  $10^4 \text{ Gpc}^{-3} \text{ yr}^{-1}$  [77].

These examples of unknown X-ray transients, whose rates in the local Universe could be comparable with that of core-collapse SNe, show how a broadband, more sensitive, survey instrument such as the ASTENA WFM-IS would significantly contribute to boost their discovery rate and to characterise them. In addition, followup observations with the ASTENA NFT would help further characterise their long-lasting emission and decay.

## ASTENA mission concept

The ASTENA in-flight configuration is shown in Fig. 7. The instrumentation on board consists of a Wide Field Monitor–Imaging Spectrometer (WFM-IS) with a 2 keV–20 MeV passband, and a Narrow Field Telescope (NFT) with a 50–600 keV passband. The WFM-IS consists of an array of 12 units, two units per each side of the hexagon, that surround the NFT. All the units are offset by 15 deg with respect to the axis of the NFT, as shown in Fig. 7. The NFT is a Laue lens telescope of about 3 m diameter and 20 m focal length. Part of the focal length (5 m) is inside the spacecraft and 15 m outside. The WFM-IS and the focal plane position sensitive detector (PSD) are inside the spacecraft at the launch. The ASTENA spacecraft can be accommodated inside the fairing of a Soyuz or Vega C launchers. Table 1 summarises the main properties of the ASTENA payload.

Table 1: Main properties of the ASTENA scientific payload.

Property \ Instrument	WFM-IS	NFT
<b>Energy passband</b>	2 keV – 20 MeV	50 – 600 keV
<b>Total useful area</b> <sup>(a)</sup>	$\sim 5800 \text{ cm}^2$ (< 30 keV) $\sim 6700 \text{ cm}^2$ (30–150 keV) $\sim 13800 \text{ cm}^2$ (> 200 keV)	7 m <sup>2</sup> (projected)
<b>Field of View</b>	2 sr	4 arcmin
<b>Angular resolution</b>	6 arcmin	$\sim 30$ arcsec HPD
<b>Point source localization accuracy</b>	1 arcmin (see text)	< 10 arcsec
<b>Minimum Detectable Polarization</b>	see Fig. 2	see Fig. 13

(a) Total geometric area through the mask or collimator.

### WFM-IS units

Each detection unit of the WFM-IS (left panel of Fig. 8) is a position sensitive detector (PSD) surmounted by a coded mask at 70 cm distance. Each couple of WFM-IS units is offset by  $15^\circ$  with respect to the NFT axis. The mask is supported by 4 Aluminum slabs with, inside, for a portion of the height, a Tungsten layer about  $500 \mu\text{m}$  thick.

### The Position Sensitive Detector unit

The PSD unit consists of an array of  $4 \times 8$  modules, each of which consists of 10 rows of hexagonal scintillator bars 4.5 mm between flats (205 bars per module), readout, on the top (toward the mask), by linear multi-anode Silicon Drift Detectors (SDDs) 0.4 mm thick, and, on the bottom, by hexagonal single anode SDDs 4.5 mm between flats (right panel of Fig. 8). The functioning

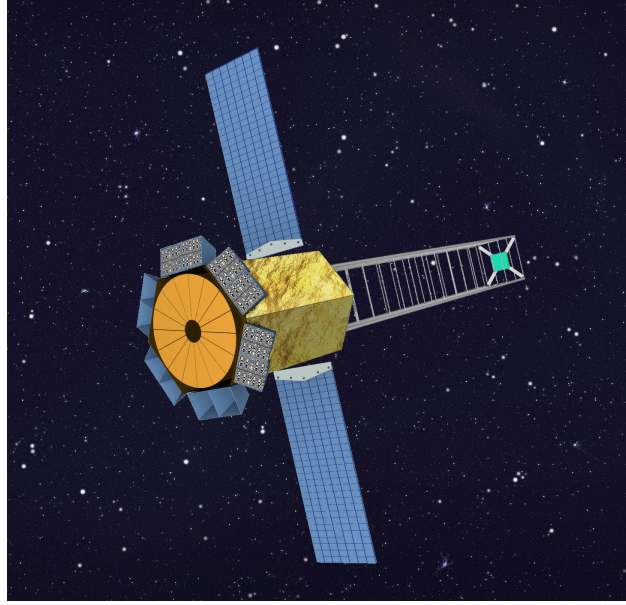


Figure 7: Artistic view of ASTENA in-flight configuration.

principle of this detector is similar to that adopted for the THESEUS XGIS [78], given its great advantage of a very broad passband (2 keV–20 MeV), a 3D position sensitivity to energy losses in the scintillator bars and a very low intrinsic background given its similarity to the phoswich system (see, e.g., Frontera et al. 79), in this case a “siswich” system as already demonstrated [80, 81]. In the case of the WFM-IS units the top SDDs have 4 linear anodes per each scintillator bar (right panel of Fig. 8). This configuration allows to get a 1D position sensitivity of 1.25 mm, which is required to achieve, with a proper coded mask (see below), a point source localisation accuracy (PSLA) of 1 arcmin at low energies ( $<30$  keV). The hexagonal cross section of the bars is crucial for giving to the instrument polarimetric capabilities (see below). In the current design the scintillator material is CsI(Tl), but also other materials (like BGO and GAGG(Ce)) will be considered. Depending on the scintillator material, the length of the bars will be optimised also for exploiting the Compton interactions in different bars for the determination of the incident photon direction.

### Coded mask

The imaging of the WFM-IS is obtained by means a double scale coded mask, one scale for the high energy photons (30–150 keV) that lose their energy in the scintillator bars, and another scale for the low energy photons ( $< 30$  keV) that lose their energy in the SDD alone. The high energy mask is made of Tungsten 1 mm thick, while the low energy mask is made of stainless steel 0.5 mm thick. The high energy mask is a  $43 \times 41$  element basic pattern of dimensions  $10 \times 10.1$  mm, with  $79 \times 79$  of such elements per each detection unit, with 50% of open 2-dimension (2D) pixels, a Fully Coded Field of View (FCFOV) of 0.27 sr, and Full Width at Zero Response (FWZR) of 2 sr. The expected PSLA is about 5 arcmin for a  $7 \sigma$  signal, and better for higher signals.

Unlike the high energy mask, the low energy mask is 1-D, with a throughput of about 65%, so as to allow the combined 2D/1D mask pattern to have a throughput of 50% at high energy and about 33% at low energy. With these properties, by positioning the 1-D directions of low energy scale of the mask of each couple (Fig. 7) perpendicularly to each other, we can achieve a PSLA of 1 arcmin,

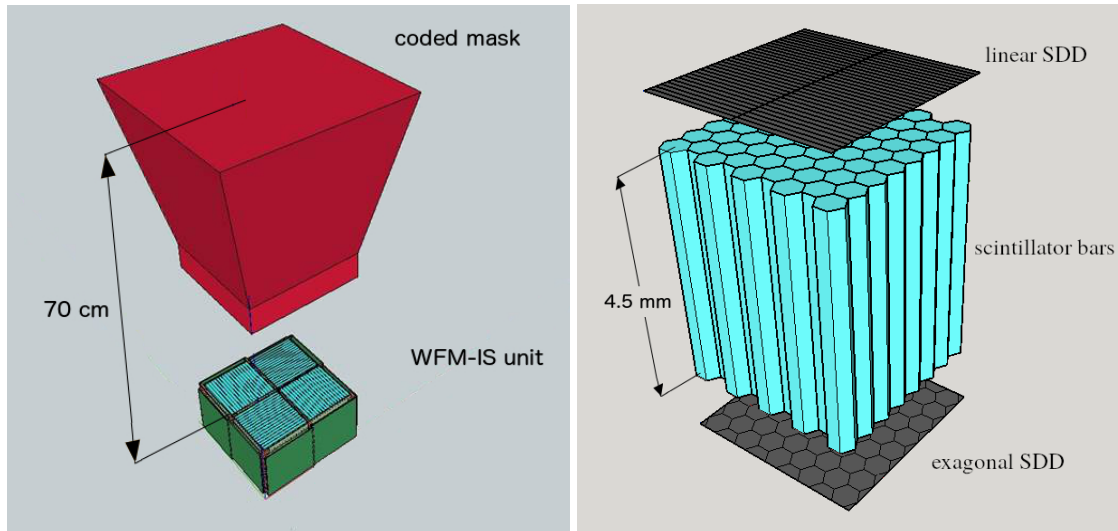


Figure 8: *Left*: a schematic view of a WFM-IS unit. *Right*: exploded view of a portion of a detection module of a WFM-IS unit.

which is required to perform NFT follow-up of sources discovered with the WFM-IS.

### WFM-IS polarimetric capabilities

Thanks to the hexagonal cross section of the scintillator bars and the 3D position sensitivity of the detector, each detection unit can be used as a Compton scattering polarimeter, as shown by the simulation results on the figure of merit (modulation factor for a 100% polarised radiation times detection efficiency for Compton interactions) and the modulation found for 100% polarised radiation of 500 keV (Fig. 9).

### WFM-IS continuum sensitivity

Considering the throughput of the coded mask, the geometric area of the WFM-IS through the mask is  $\sim 5800 \text{ cm}^2$  below 30 keV and  $7000 \text{ cm}^2$  in 30–150 keV. At higher energies the mask is transparent to the radiation therefore the on-axis area is about  $1.4 \text{ m}^2$ . Assuming the background level expected for a nearly equatorial orbit, Figure 10 shows the WFM-IS continuum sensitivity as a function of the exposure time for a source in the FOV of the NFT.

### Narrow Field Telescope, NFT

The NFT is based on a broadband (50–600 keV) Laue lens with  $\sim 3 \text{ m}$  diameter and 20 m focal length (left panel of in Fig. 11), with a PSD in the focal plane. In the following we separately discuss both, Laue lens and PSD.

### Laue lens

For a review on the basic principles underlying Laue lenses, see [82]. Briefly, Laue lenses exploit the crystal diffraction in transmission configuration (Laue geometry). A Laue lens is made of a large number of crystal tiles in transmission configuration, that are disposed so as to focus the incident radiation onto a common focal spot. A convenient way to visualise the crystal lens is considering it as a spherical cup covered up with rings of crystal tiles having their diffracting planes perpendicular to the spherical surface, with the focal spot on the symmetry axis at a distance  $f = R/2$  from the

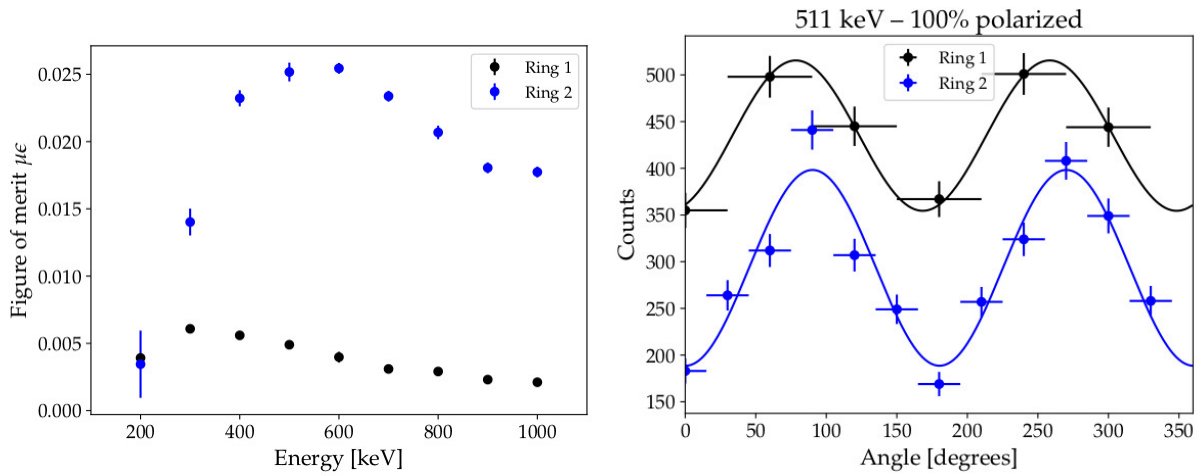


Figure 9: *Left*: figure of merit for polarised radiation (see text). *Right*: Modulation of the 511 keV polarised radiation scattered from the first and second ring around a generic pixel.

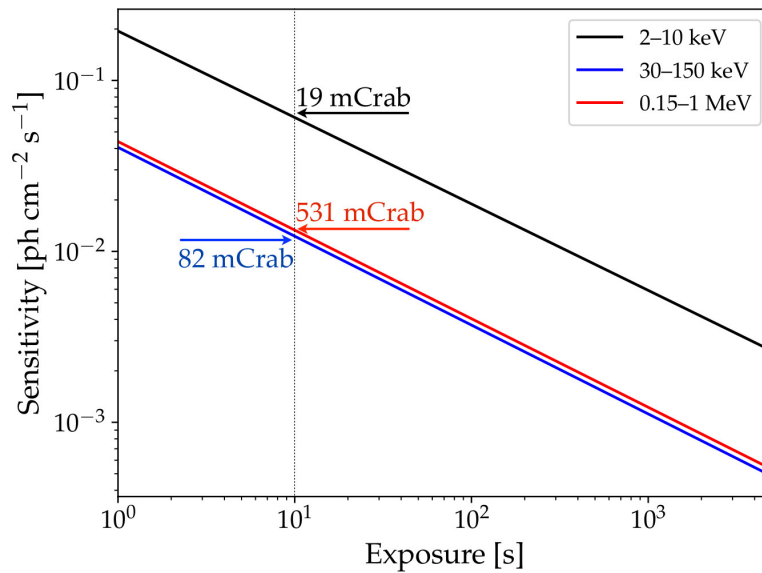


Figure 10: Continuum sensitivity of the WFM-IS in three energy bands, in the case of a source in the FOV of all detection units.

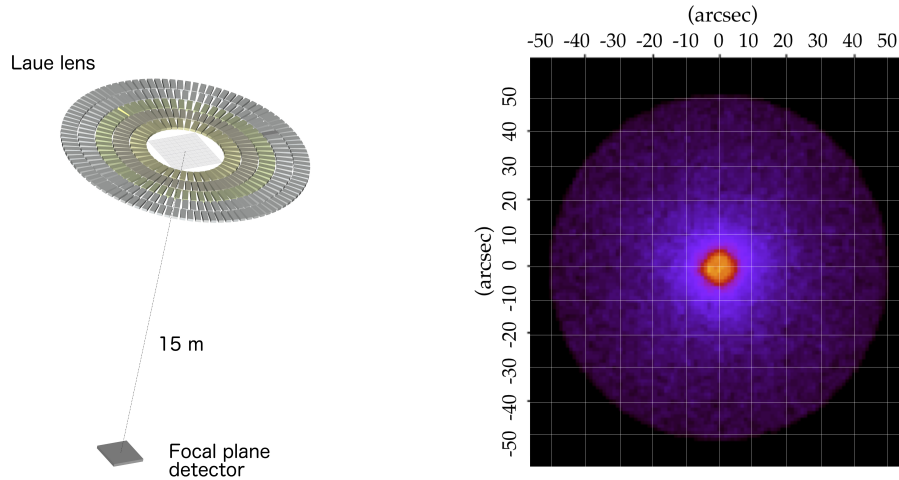


Figure 11: *Left*: Sketch of the Laue lens adopted for the ASTENA NFT which will be made of bent crystals. *Right*: 2-D PSF for an on-axis source achieved with the NFT using diffractive bent crystals.

cup ( $R$  is the curvature radius of the spherical cup). From the Bragg law and the geometry of the lens, the reflected energy from a crystal at distance  $r$  from the lens symmetry axis is [82]

$$E = \frac{hc}{2d_{hkl}} \sin \left[ \frac{1}{2} \arctan \left( \frac{f}{r} \right) \right] \approx \frac{hc f}{d_{hkl} r},$$

where  $d_{hkl}$  (in  $\text{\AA}$ ) is the distance between the chosen lattice planes ( $hkl$  Miller indices) of the crystals,  $hc = 12.4 \text{ keV}\cdot\text{\AA}$  and  $E$  is the energy of the  $\gamma$ -ray photon (in keV). The approximated expression is valid for  $\gamma$ -ray lenses, given the small diffraction angles involved. Thus, the highest (lowest) energies are diffracted from the nearest (furthest) crystals to the lens axis. At the University of Ferrara, with the project HAXTEL (Hard X-ray TELEscope) we developed a technology for assembling Laue lenses with  $< 10$ -m focal length, using flat mosaic crystal tiles of Cu(111) [83, 84].

The disadvantage of flat crystals is that the minimum focal spot size is that of the crystal tiles. To overcome this limitation, bent crystals with the proper curvature are required. To this end, a technology for bending crystals and for assembling a Laue lens with long focal length (20 m) for astrophysical applications, was successfully developed as part of the LAUE project supported by the Italian Space Agency (ASI) [85]. With the support of the AHEAD project, the expected performance of a Laue lens prototype has also been simulated taking into account effects of possible crystal tile misalignments and radial distortions of the crystal curvature.

Bent crystals have been produced and a technology for an accurate alignment (the requirement is a misalignment  $< 10$  arcsec) of the crystal tiles in the lens has been identified [86] with successful results (paper in preparation). The development of a lens prototype is the goal of a recently approved project TRILL (Technological Readiness level Increase for Laue Lenses) devoted to increase the Technology Readiness Level (TRL). The ASTENA NFT builds upon these results. The expected PSF of the lens is shown in Figure 11, with a Half Energy Width (HEW) of 30 arcsec.

Key features of the proposed lens are its energy passband, angular resolution, and FOV. Thanks to the use of bent Si(111) and Ge(111), the energy passband 50–600 keV is guaranteed, but we will explore the possibility to extend the energy band down to 30 keV, if the transparency of the passive materials in the lens under the crystals is still acceptable.

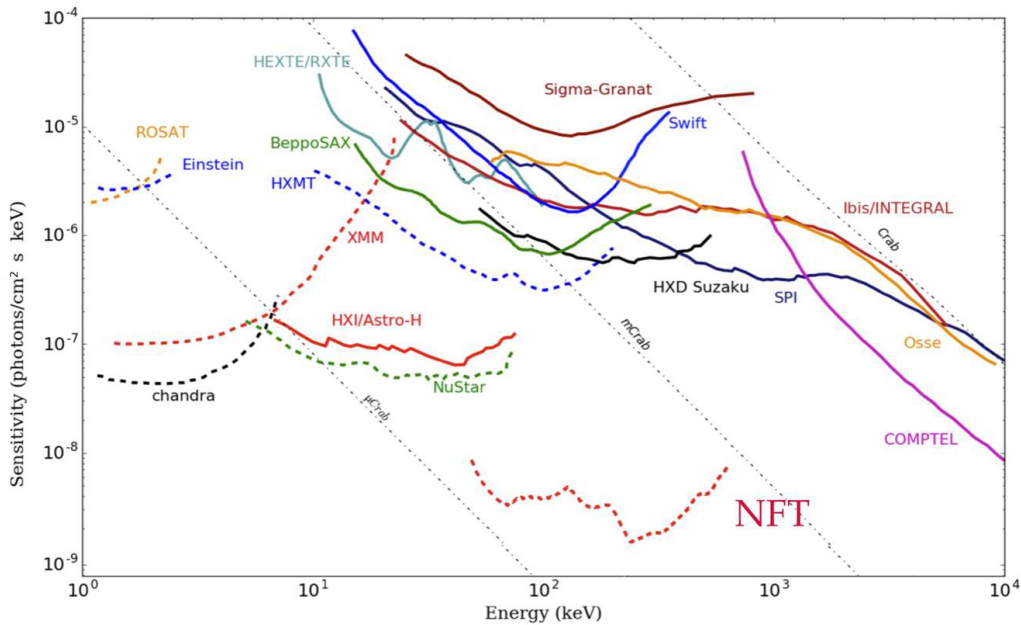


Figure 12: NFT continuum sensitivity at  $3\sigma$ , with  $\Delta E = E/2$  and  $\Delta T = 10^5$  s.

### Focal plane detector

The focal-plane detector is a solid state PSD made of 4 layers, with each layer made of  $4 \times 16$  CdZnTe (CZT) elements. The PSD has a total cross section of  $8 \times 8$  cm<sup>2</sup> and a total thickness of 8 cm, so as to have a detection efficiency higher than 80% in the entire NFT energy band. The measured 3-D position resolution of a single element is already that required by the ASTENA NFT: 300  $\mu$ m [87, 88]. In this configuration, the PSD can work as a Compton polarimeter [89].

### Expected NFT performance

- Sensitivity to continuum emission.** The expected NFT continuum sensitivity ( $3\sigma$ ,  $10^5$  s,  $\Delta E = E/2$ ) is shown in Fig. 12, compared with that of other experiments. Thanks to the photon reflection in transmission geometry, the lens projected geometric area is  $\sim 7$  m<sup>2</sup>, with a very low mass ( $\sim 150$  kg). Comparison with the NASA Medium Probe design mission AMEGO [90], not shown in Fig. 12, the expected ASTENA sensitivity is at least two orders of magnitude better than that of AMEGO with the same exposure.
- Sensitivity to polarised radiation.** Thanks to an unprecedented sensitivity (up to two orders of magnitude better than operating instruments in the same energy band), together with the focal plane characteristics (high segmentation, spatial resolution in 3D and good spectroscopy) the NFT will contribute to turn polarimetry into a standard observation mode between 100 and 600/700 keV. Figure 13 shows the estimated MDP as a function of both the observing time for a 10 mCrab source, and the source intensity integrated over a measurement time of  $10^5$  s, assuming for the source a Crab-like spectrum and the background estimate given by Dean et al. [91] and later confirmed with the *INTEGRAL*/SPI instrument, scaled to a low earth orbit. The results confirm very good polarimetry performance of the NFT telescope with an achievable MDP of 5% for a 10mCrab source for a  $10^5$  s observation time.

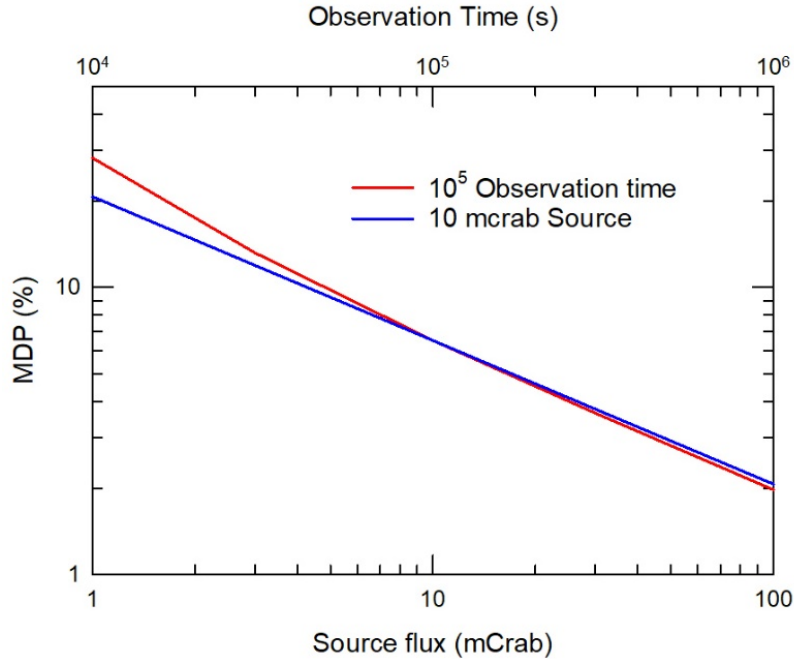


Figure 13: Minimum Detectable polarisation (MDP) in  $10^5$  s as a function of the polarised source intensity (*red line*) and for a 10-mCrab source as a function of the observation time (*blue line*).

- Sensitivity to narrow emission lines.** At  $3\sigma$  confidence, for the case of a Laue lens with Gaussian distribution of the radial distortion within 2.5% and a tile misalignment within 10 arcsec, the sensitivity to emission lines shown in Fig. 14 for an exposure of  $10^5$  s, a continuum intensity given by our sensitivity to continuum, a FWHM of the line of 2 keV and the fraction  $f_\varepsilon = 0.5$ , corresponding to a half energy width of the PSF. As can be seen, the sensitivity to lines in  $10^5$  s is about three orders of magnitude better than the *INTEGRAL/SPI* instrument at low energy, while it is about one order of magnitude better at 511 keV. This sensitivity can be further improved through a suitable choice of the reflecting planes of bent crystals. Comparison with the NASA Medium Probe design mission AMEGO [90] in the common passband shows a much higher sensitivity of ASTENA at low energies, while at 511 keV is similar, but with an order of magnitude better angular resolution of ASTENA.

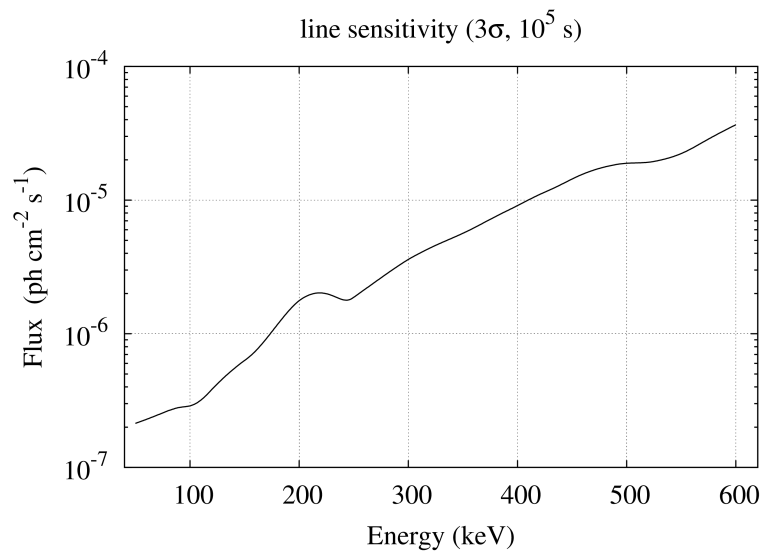


Figure 14: Expected line sensitivity ( $3\sigma$  confidence) for the ASTENA-NFT, calculated for a  $10^5$ -s exposure.



## Bibliography

- [1] P. Kumar and B. Zhang, *Phys. Rep.* **561**, 1 (2015), 1410.0679.
- [2] E. Costa, F. Frontera, J. Heise, M. Feroci, J. in't Zand, F. Fiore, M. N. Cinti, D. Dal Fiume, L. Nicastro, M. Orlandini, et al., *Nature* **387**, 783 (1997), astro-ph/9706065.
- [3] J. Granot, T. Piran, O. Bromberg, J. L. Racusin, and F. Daigne, *Space Science Reviews* (2015), 1507.08671.
- [4] L. Sironi and A. Spitkovsky, *ApJ* **741**, 39 (2011), 1107.0977.
- [5] D. Lazzati, *X-ray polarization of gamma-ray bursts, from X-ray Polarimetry: A New Window in Astrophysics* by Ronaldo Bellazzini, Enrico Costa, Giorgio Matt and Gianpiero Tagliaferri, Cambridge University Press (2010), p. 202.
- [6] C. G. Mundell, I. A. Steele, R. J. Smith, S. Kobayashi, A. Melandri, C. Guidorzi, A. Gomboc, C. J. Mottram, D. Clarke, A. Monfardini, et al., *Science* **315**, 1822 (2007), arXiv:astro-ph/0703654.
- [7] I. A. Steele, C. G. Mundell, R. J. Smith, S. Kobayashi, and C. Guidorzi, *Nature* **462**, 767 (2009), 1010.1255.
- [8] C. G. Mundell, D. Kopac, D. M. Arnold, I. A. Steele, A. Gomboc, S. Kobayashi, R. M. Harrison, R. J. Smith, C. Guidorzi, F. J. Virgili, et al., *Nature* **504**, 119 (2013).
- [9] E. Troja, V. M. Lipunov, C. G. Mundell, N. R. Butler, A. M. Watson, S. Kobayashi, S. B. Cenko, F. E. Marshall, R. Ricci, A. Fruchter, et al., *Nature* **547**, 425 (2017).
- [10] M. L. McConnell, *New A Rev.* **76**, 1 (2017), 1611.06579.
- [11] S.-N. Zhang, M. Kole, T.-W. Bao, T. Batsch, T. Bernasconi, F. Cadoux, J.-Y. Chai, Z.-G. Dai, Y.-W. Dong, N. Gauvin, et al., *Nature Astronomy* **3**, 258 (2019), 1901.04207.
- [12] M. Lyutikov, V. I. Pariev, and R. D. Blandford, *ApJ* **597**, 998 (2003), astro-ph/0305410.
- [13] D. Lazzati, E. Rossi, G. Ghisellini, and M. J. Rees, *MNRAS* **347**, L1 (2004), astro-ph/0309038.

- 
- [14] K. Toma, T. Sakamoto, B. Zhang, J. E. Hill, M. L. McConnell, P. F. Bloser, R. Yamazaki, K. Ioka, and T. Nakamura, *ApJ* **698**, 1042 (2009), 0812.2483.
- [15] B. Zhang and H. Yan, *ApJ* **726**, 90 (2011), 1011.1197.
- [16] J.-J. Wei and X.-F. Wu, *Phys. Rev. D* **99**, 103012 (2019), 1905.09995.
- [17] B. P. Abbott, R. Abbott, T. D. Abbott, F. Acernese, K. Ackley, C. Adams, T. Adams, P. Addesso, R. X. Adhikari, V. B. Adya, et al., *ApJ* **848**, L12 (2017), 1710.05833.
- [18] S. Nissanke, D. E. Holz, S. A. Hughes, N. Dalal, and J. L. Sievers, *ApJ* **725**, 496 (2010), 0904.1017.
- [19] C. Guidorzi, R. Margutti, D. Brout, D. Scolnic, W. Fong, K. D. Alexander, P. S. Cowperthwaite, J. Annis, E. Berger, and et al., *ApJ* **851**, L36 (2017), 1710.06426.
- [20] G. Amelino-Camelia, J. Ellis, N. E. Mavromatos, D. V. Nanopoulos, and S. Sarkar, *Nature* **395**, 525 (1998).
- [21] A. Goldstein, P. Veres, E. Burns, M. S. Briggs, R. Hamburg, D. Kocevski, C. A. Wilson-Hodge, R. D. Preece, S. Poolakkil, and et al., *ApJ* **848**, L14 (2017), 1710.05446.
- [22] T. P. Li, S. Xiong, S. Zhang, F. Lu, L. Song, X. Cao, Z. Chang, G. Chen, L. Chen, and et al., *Science China Physics, Mechanics, and Astronomy* **61**, 31011 (2018), 1710.06065.
- [23] O. S. Salafia, G. Ghirlanda, S. Ascenzi, and G. Ghisellini, arXiv e-prints arXiv:1905.01190 (2019), 1905.01190.
- [24] O. S. Salafia, G. Ghisellini, A. Pescalli, G. Ghirlanda, and F. Nappo, *MNRAS* **450**, 3549 (2015), 1502.06608.
- [25] A. Pescalli, G. Ghirlanda, O. S. Salafia, G. Ghisellini, F. Nappo, and R. Salvaterra, *MNRAS* **447**, 1911 (2015), 1409.1213.
- [26] M. Punturo, H. Lück, and M. Beker, in *Advanced Interferometers and the Search for Gravitational Waves*, edited by M. Bassan (2014), vol. 404 of *Astrophysics and Space Science Library*, p. 333.
- [27] C. Barbieri, O. S. Salafia, A. Perego, M. Colpi, and G. Ghirlanda, *A&A* **625**, A152 (2019), 1903.04543.
- [28] A. Sesana, *Phys. Rev. Lett.* **116**, 231102 (2016), 1602.06951.
- [29] R. Willingale and P. Mészáros, *Space Sci. Rev.* **207**, 63 (2017).
- [30] E. Maiorano, N. Masetti, E. Palazzi, F. Frontera, P. Grandi, and et al., *Astronomy and Astrophysics* **438**, 821 (2005), arXiv:astro-ph/0504602.
- [31] C. Kouveliotou, J. Granot, J. L. Racusin, E. Bellm, G. Vianello, S. Oates, C. L. Fryer, S. E. Boggs, F. E. Christensen, W. W. Craig, et al., *ApJ* **779**, L1 (2013), 1311.5245.

- 
- [32] A. Martin-Carrillo, L. Hanlon, M. Topinka, A. P. LaCluyzé, V. Savchenko, D. A. Kann, A. S. Trotter, S. Covino, T. Krühler, and J. Greiner, *A&A* **567**, A84 (2014), 1405.7396.
- [33] A. Corsi, L. Piro, E. Kuulkers, L. Amati, L. A. Antonelli, and et al., *Astronomy and Astrophysics* **438**, 829 (2005), [arXiv:astro-ph/0504607](#).
- [34] A. Moretti, R. Margutti, F. Pasotti, A. P. Beardmore, S. Campana, G. Chincarini, S. Covino, O. Godet, C. Guidorzi, J. P. Osborne, et al., *A&A* **478**, 409 (2008).
- [35] R. Margutti, C. Guidorzi, D. Lazzati, D. Milisavljevic, A. Kamble, T. Laskar, J. Parrent, N. C. Gehrels, and A. M. Soderberg, *ApJ* **805**, 159 (2015), 1410.7387.
- [36] G. Ghisellini, G. Ghirlanda, L. Nava, and A. Celotti, *MNRAS* **403**, 926 (2010), 0910.2459.
- [37] R. Barniol Duran and P. Kumar, *MNRAS* **412**, 522 (2011), 1003.5916.
- [38] M. Ajello, M. Arimoto, M. Axelsson, L. Baldini, G. Barbiellini, D. Bastieri, R. Bellazzini, P. N. Bhat, E. Bissaldi, R. D. Blandford, et al., *ApJ* **878**, 52 (2019), 1906.11403.
- [39] M. Ajello, L. Baldini, G. Barbiellini, D. Bastieri, R. Bellazzini, E. Bissaldi, R. D. Blandford, R. Bonino, E. Bottacini, and J. Bregeon, *ApJ* **863**, 138 (2018).
- [40] A. M. Beloborodov, R. Hascoët, and I. Vurm, *ApJ* **788**, 36 (2014), 1307.2663.
- [41] S. Campana, V. Mangano, A. J. Blustin, P. Brown, D. N. Burrows, G. Chincarini, J. R. Cummings, G. Cusumano, M. Della Valle, and et al., *Nature* **442**, 1008 (2006), [astro-ph/0603279](#).
- [42] J. P. U. Fynbo, D. Watson, C. C. Thöne, J. Sollerman, J. S. Bloom, and et al., *Nature* **444**, 1047 (2006), [astro-ph/0608313](#).
- [43] R. Margutti, A. M. Soderberg, M. H. Wieringa, P. G. Edwards, R. A. Chevalier, B. J. Morsony, R. Barniol Duran, L. Sironi, B. A. Zauderer, D. Milisavljevic, et al., *ApJ* **778**, 18 (2013), 1308.1687.
- [44] E. Nakar and R. Sari, *ApJ* **747**, 88 (2012), 1106.2556.
- [45] S. R. Kulkarni, D. A. Frail, M. H. Wieringa, R. D. Ekers, E. M. Sadler, R. M. Wark, J. L. Higdon, E. S. Phinney, and J. S. Bloom, *Nature* **395**, 663 (1998).
- [46] E. Pian, L. Amati, L. A. Antonelli, R. C. Butler, E. Costa, G. Cusumano, J. Danziger, M. Feroci, F. Fiore, F. Frontera, et al., *ApJ* **536**, 778 (2000), [astro-ph/9910235](#).
- [47] A. M. Soderberg, S. R. Kulkarni, E. Nakar, E. Berger, P. B. Cameron, and et al., *Nature* **442**, 1014 (2006), [astro-ph/0604389](#).
- [48] D. Guetta and M. Della Valle, *ApJ* **657**, L73 (2007), [astro-ph/0612194](#).
- [49] E. Liang, B. Zhang, F. Virgili, and Z. G. Dai, *ApJ* **662**, 1111 (2007), [astro-ph/0605200](#).

- 
- [50] M. R. Drout, R. Chornock, A. M. Soderberg, N. E. Sanders, R. McKinnon, A. Rest, R. J. Foley, D. Milisavljevic, R. Margutti, E. Berger, et al., *ApJ* **794**, 23 (2014), 1405.3668.
- [51] M. Pursiainen, M. Childress, M. Smith, S. Prajs, M. Sullivan, T. M. Davis, R. J. Foley, J. Asorey, J. Calcino, D. Carollo, et al., *MNRAS* **481**, 894 (2018), 1803.04869.
- [52] A. Rest, P. M. Garnavich, D. Khatami, D. Kasen, B. E. Tucker, E. J. Shaya, R. P. Olling, R. Mushotzky, A. Zenteno, S. Margheim, et al., *Nature Astronomy* **2**, 307 (2018), 1804.04641.
- [53] S. J. Smartt, P. Clark, K. W. Smith, O. McBrien, K. Maguire, D. O’Neil, M. Fulton, M. Magee, S. Prentice, C. Colin, et al., *The Astronomer’s Telegram* **11727** (2018).
- [54] R. Margutti, B. D. Metzger, R. Chornock, I. Vurm, N. Roth, B. W. Grefenstette, V. Savchenko, R. Cartier, J. F. Steiner, G. Terreran, et al., *ApJ* **872**, 18 (2019).
- [55] K. Morokuma-Matsui, T. Morokuma, N. Tominaga, B. Hatsukade, M. Hayashi, Y. Tamura, Y. Matsuda, K. Motogi, K. Niinuma, and M. Konishi, *ApJ* **879**, L13 (2019), 1906.05446.
- [56] D. R. Lorimer, M. Bailes, M. A. McLaughlin, D. J. Narkevic, and F. Crawford, *Science* **318**, 777 (2007), 0709.4301.
- [57] E. Petroff, J. W. T. Hessels, and D. R. Lorimer, *The Astronomy and Astrophysics Review* **27**, 4 (2019), ISSN 1432-0754, URL <https://doi.org/10.1007/s00159-019-0116-6>.
- [58] J. I. Katz, *Progress in Particle and Nuclear Physics* **103**, 1 (2018), 1804.09092.
- [59] L. G. Spitler, P. Scholz, J. W. T. Hessels, S. Bogdanov, A. Brazier, F. Camilo, S. Chatterjee, J. M. Cordes, F. Crawford, and et al., *Nature* **531**, 202 (2016), 1603.00581.
- [60] S. Chatterjee, C. J. Law, R. S. Wharton, S. Burke-Spolaor, J. W. T. Hessels, G. C. Bower, J. M. Cordes, S. P. Tendulkar, C. G. Bassa, P. Demorest, et al., *Nature* **541**, 58 (2017), 1701.01098.
- [61] S. P. Tendulkar, C. G. Bassa, J. M. Cordes, G. C. Bower, C. J. Law, S. Chatterjee, E. A. K. Adams, S. Bogdanov, S. Burke-Spolaor, B. J. Butler, et al., *ApJ* **834**, L7 (2017), 1701.01100.
- [62] K. W. Bannister, A. T. Deller, C. Phillips, J. P. Macquart, J. X. Prochaska, N. Tejos, S. D. Ryder, E. M. Sadler, R. M. Shannon, and S. Simha, *arXiv e-prints arXiv:1906.11476* (2019), 1906.11476.
- [63] V. Ravi, M. Catha, L. D’Addario, S. G. Djorgovski, G. Hallinan, R. Hobbs, J. Kocz, S. R. Kulkarni, J. Shi, and H. K. Vedantham, *arXiv e-prints arXiv:1907.01542* (2019), 1907.01542.
- [64] The CHIME/FRB Collaboration, :, M. Amiri, K. Bandura, M. Bhardwaj, P. Boubel, M. M. Boyce, P. J. Boyle, C. Brar, M. Burhanpurkar, et al., *arXiv e-prints* (2019), 1901.04525.
- [65] J. J. DeLaunay, D. B. Fox, K. Murase, P. Mészáros, A. Keivani, C. Messick, M. A. Mostafá, F. Oikonomou, G. Tešić, and C. F. Turley, *ApJ* **832**, L1 (2016), 1611.03139.
- [66] S. P. Tendulkar, V. M. Kaspi, and C. Patel, *ApJ* **827**, 59 (2016), 1602.02188.

- 
- [67] P. Scholz, S. Bogdanov, J. W. T. Hessels, R. S. Lynch, L. G. Spitler, C. G. Bassa, G. C. Bower, S. Burke-Spolaor, B. J. Butler, S. Chatterjee, et al., *ApJ* **846**, 80 (2017), 1705.07824.
- [68] C. Guidorzi, M. Marongiu, R. Martone, L. Amati, F. Frontera, L. Nicastro, M. Orlandini, R. Margutti, and E. Virgilli, arXiv e-prints arXiv:1907.08386 (2019), 1907.08386.
- [69] K. Murase, K. Kashiyama, and P. Mészáros, *MNRAS* **461**, 1498 (2016), 1603.08875.
- [70] K. Murase, P. Mészáros, and D. B. Fox, *ApJ* **836**, L6 (2017), 1611.03848.
- [71] B. Zhang, *ApJ* **836**, L32 (2017), 1701.04094.
- [72] B. D. Metzger, B. Margalit, and L. Sironi, *MNRAS* **485**, 4091 (2019), 1902.01866.
- [73] P. G. Jonker, A. Glennie, M. Heida, T. Maccarone, S. Hodgkin, G. Nelemans, J. C. A. Miller-Jones, M. A. P. Torres, and R. Fender, *ApJ* **779**, 14 (2013), 1310.7238.
- [74] B. Luo, W. N. Brandt, and F. Bauer, *The Astronomer's Telegram* **6625**, 1 (2014).
- [75] A. Glennie, P. G. Jonker, R. P. Fender, T. Nagayama, and M. L. Pretorius, *MNRAS* **450**, 3765 (2015), 1504.03720.
- [76] J. A. Irwin, W. P. Maksym, G. R. Sivakoff, A. J. Romanowsky, D. Lin, T. Speegle, I. Prado, D. Mildebrath, J. Strader, J. Liu, et al., *Nature* **538**, 356 (2016), 1610.05781.
- [77] F. E. Bauer, E. Treister, K. Schawinski, S. Schulze, B. Luo, D. M. Alexander, W. N. Brandt, A. Comastri, F. Forster, R. Gilli, et al., *MNRAS* **467**, 4841 (2017), 1702.04422.
- [78] R. Campana, F. Fuschino, C. Labanti, L. Amati, S. Mereghetti, M. Fiorini, F. Frontera, G. Baldazzi, P. Bellutti, and et al., *Mem. Soc. Astron. Italiana* **89**, 137 (2018), 1802.01674.
- [79] F. Frontera, E. Costa, D. dal Fiume, M. Feroci, L. Nicastro, M. Orlandini, E. Palazzi, and G. Zavattini, *Astronomy and Astrophysics Suppl. Series* **122**, 357 (1997).
- [80] M. Marisaldi, C. Labanti, and H. Soltau, *IEEE Transactions on Nuclear Science* **51**, 1916 (2004).
- [81] M. Marisaldi, C. Labanti, H. Soltau, C. Fiorini, A. Longoni, and F. Perotti, *IEEE Transactions on Nuclear Science* **52**, 1842 (2005).
- [82] F. Frontera and P. von Ballmoos, *X-Ray Optics and Instrumentation, 2010. Special Issue on X-Ray Focusing: Techniques and Applications*, id.215375 **2010**, 215375 (2010), 1007.4308.
- [83] F. Frontera, G. Loffredo, A. Pisa, F. Nobili, V. Carassiti, F. Evangelisti, L. Landi, S. Squerzanti, E. Caroli, J. B. Stephen, et al., in *Society of Photo-Optical Instrumentation Engineers (SPIE) Conference Series* (2008), vol. 7011.
- [84] E. Virgilli, F. Frontera, V. Valsan, V. Liccardo, V. Carassiti, F. Evangelisti, and S. Squerzanti, in *Society of Photo-Optical Instrumentation Engineers (SPIE) Conference Series* (2011), vol. 8147 of *Proc. SPIE*, p. 81471B, 1110.5493.

- [85] E. Virgili, V. Valsan, F. Frontera, E. Caroli, V. Liccardo, and J. B. Stephen, *Journal of Astronomical Telescopes, Instruments, and Systems* **3**, 044001 (2017), 1711.03475.
- [86] E. Virgili, F. Frontera, P. Rosati, V. Liccardo, S. Squerzanti, V. Carassiti, E. Caroli, N. Auricchio, and J. B. Stephen, in *Society of Photo-Optical Instrumentation Engineers (SPIE) Conference Series* (2015), vol. 9603 of *Proc. SPIE*, p. 960308, 1509.03416.
- [87] I. Kuvvetli, C. Budtz-Jørgensen, E. Caroli, and N. Auricchio, *Nuclear Instruments and Methods in Physics Research A* **624**, 486 (2010).
- [88] I. Kuvvetli, C. Budtz-Jørgensen, A. Zappettini, N. Zambelli, G. Benassi, E. Kalemci, E. Caroli, J. B. Stephen, and N. Auricchio, in *High Energy, Optical, and Infrared Detectors for Astronomy VI* (2014), vol. 9154 of *Proc. SPIE*, p. 91540X.
- [89] E. Caroli, M. Moita, R. da Silva, S. Del Sordo, G. de Cesare, J. Maia, and M. Pàscoa, *Galaxies* **6**, 69 (2018).
- [90] J. McEnery, J. Abel Barrio, I. Agudo, M. Ajello, J.-M. Álvarez, S. Ansoldi, S. Anton, and et al., arXiv e-prints arXiv:1907.07558 (2019), 1907.07558.
- [91] A. J. Dean, L. Fan, K. Byard, A. Goldwurm, and C. J. Hall, *A&A* **219**, 358 (1989).